


Research Article

Open Access



Study on the performance of lead zirconate titanate piezoelectric coating prepared by vacuum cold spraying

Hefa Zhu^{1,2}, Yanfei Huang², Weiling Guo², Han Dong¹, Zhiguo Xing² , Qingbo Mi³

¹School of Materials Science and Engineering, Shanghai University, Shanghai 200444, China.

²National Key Lab for Remanufacturing, Army Academy of Armored Forces, Beijing 100072, China.

³AECC Harbin Dongan Engine Co., LTD. Harbin 150066, Heilongjiang, China.

Correspondence to: Dr. Han Dong, School of Materials Science and Engineering, Shanghai University, No. 99 Shangda Road, Baoshan District, Shanghai 200444, China. E-mail: 1245020695@qq.com; Dr. Zhiguo Xing, National Key Lab for Remanufacturing, Army Academy of Armored Forces, 21 Dujikan, Fengtai District, Beijing 100072, China. E-mail: xingzg2011@163.com

How to cite this article: Zhu H, Huang Y, Guo W, Dong H, Xing Z, Mi Q. Study on the performance of lead zirconate titanate piezoelectric coating prepared by vacuum cold spraying. *Green Manuf Open* 2023;1:13. <https://dx.doi.org/10.20517/gmo.2023.05>

Received: 1 Jun 2023 **First Decision:** 16 Aug 2023 **Revised:** 10 Sep 2023 **Accepted:** 21 Sep 2023 **Published:** 25 Sep 2023

Academic Editors: Hongchao Zhang, Zhichao Liu **Copy Editor:** Dong-Li Li **Production Editor:** Dong-Li Li

Abstract

By utilizing the force-electric conversion capabilities of piezoelectric materials, piezoelectric ceramic coatings are intended to monitor the state of component damage. In this study, lead zirconate titanate [Pb(Zr, Ti)O₃, PZT] piezoelectric ceramic coatings were prepared on the SUS304 substrate by vacuum cold spraying (VCS). The phase structure, microstructure, and electrical properties of the PZT coating were analyzed. According to the findings, the PZT coating has a typical tetragonal perovskite structure, and the Xi photoelectron spectrometer (XPS) findings show that the room-temperature deposition characteristics of VCS techniques do not affect the elemental valence state of PZT materials, making it a non-destructive way to create the coating. The surface of the PZT coating is uniform and smooth, and the surface roughness Ra is about 195 nm. The PZT coating has a microhardness of around 1,510 Hv and an elastic modulus of about 73.9 GPa. Meanwhile, the piezoelectric coefficient d₃₃ of the PZT coating was about 46 pC/N. The maximum saturation polarization of the PZT coating was 16.2 μC/cm², the remnant polarization was 3.1 μC/cm², and the coercive field was 59.3 kV/cm, which showed some ferroelectricity. The dielectric constant/dielectric loss of the PZT coating was about 425/0.35. The Curie temperature of PZT coating is 392.6 °C, which improves the application temperature range of PZT coating. This demonstrates that the PZT coatings created by VCS have certain electrical capabilities, offering a novel way to create and enhance the piezoelectric ceramic coating system for later-stage part monitoring.

Keywords: Lead zirconate titanate, vacuum cold spraying, ferroelectric properties, dielectric properties



© The Author(s) 2023. **Open Access** This article is licensed under a Creative Commons Attribution 4.0 International License (<https://creativecommons.org/licenses/by/4.0/>), which permits unrestricted use, sharing, adaptation, distribution and reproduction in any medium or format, for any purpose, even commercially, as long as you give appropriate credit to the original author(s) and the source, provide a link to the Creative Commons license, and indicate if changes were made.



INTRODUCTION

Remanufacturing is an eco-friendly, energy-efficient, and environmentally friendly method^[1]. Surface coating technology is a key developed technique in remanufacturing^[2]. Existing equipment parts are prone to fatigue damage and other problems during use, thus affecting the service life of the parts. Therefore, the establishment of a timely and accurate monitoring system plays a vital role in the long-life use of parts^[3]. Therefore, one of the key techniques to implement component health monitoring is the creation of piezoelectric ceramic coating^[4,5]. Due to its stable physicochemical characteristics^[6,7] and superior piezoelectric, ferroelectric, and dielectric capabilities^[8,9], lead zirconate titanate [Pb(Zr, Ti)O₃, PZT] material is a crucial option for achieving the aforementioned tasks. PZT is a continuous solid solution of PbTiO₃ and PbZrO₃ in any ratio to generate different properties^[10,11], and its lattice structure is an ABO₃-type Perovskite structure. The electromechanical coupling coefficient, piezoelectric constant, and dielectric constant of the PZT material in this component reach their maximum values when the ratio of Zr to Ti is 52:48 due to the phase instability, which is known as the morphotropic phase boundary (MPB) under this ratio^[12,13].

PZT ceramics are typically prepared using techniques such as plasma spraying^[14], magnetron sputtering^[15], sol-gel methods^[16], and vacuum cold spraying (VCS)^[17]. In the 1990s, the first VCS technology was created. By using the Aerosol deposition (AD) method, Akedo *et al.* effectively created PZT piezoelectric thickness for the first time on different substrate surfaces^[18]. The method depends on the impact adhesion deposition of ultrafine powder particles on the substrate surface while under vacuum to prepare the coating. The coating deposition technique was also given the moniker Nanoparticle deposition system (NPDS) by Chun *et al.*^[19]. The operating concepts of coating preparation by air floating deposition and coating preparation by cold spraying are similar, in addition to coating preparation in a vacuum environment^[20]. As a result, the VCS system was independently created and prepared by the thermal spray lab at Xi'an Jiaotong University. VCS is a novel method for thin film deposition at room temperature. When spraying, the nozzle accelerates ultrafine powder particles, allowing them to collide quickly with the substrate or film surface. This causes plastic deformation and fracture, and the film is then produced by the tamping impact of succeeding particles^[21,22]. VCS, when compared to conventional thin film preparation techniques, has the benefits of low deposition temperature, high deposition rate, high film densities, a wide variety of substrates, and wide film thicknesses^[23].

In short, it offers specific advantages for the creation of piezoelectric ceramic coatings because of the properties of vacuum deposition at room temperature by VCS. In this paper, the forming mechanism of VCS PZT coating was studied, and the changes of phase structure, microstructure, and electrical properties of PZT coating were analyzed, which laid a solid foundation for the preparation of piezoelectric ceramic coating for monitoring the state of parts.

METHODS

Characterization and measurements

Adopting PM100L planetary ball mill for ball milling of PZT powder to achieve the particle size of the powder to meet the spraying requirements. An MRA3LMH scanning electron microscopy (SEM) with secondary electrons was used to observe the morphology of the powder, coating surface, and cross-section. Using a Mastersizer 2000 laser particle size scattering device, the particle size distribution of the powders both before and after ball milling was evaluated. A Bruker D8 ADVANCE X-ray diffractometer (XRD) was used to test and analyze the phase structure of the PZT powders and coatings. Thermo Scientific Escalab 250 Xi photoelectron spectrometer (XPS) with 250 Xi from Thermo Fisher, USA, was used for the energy test of X-ray photons in order to evaluate the chemical state and surface composition of the PZT coatings.

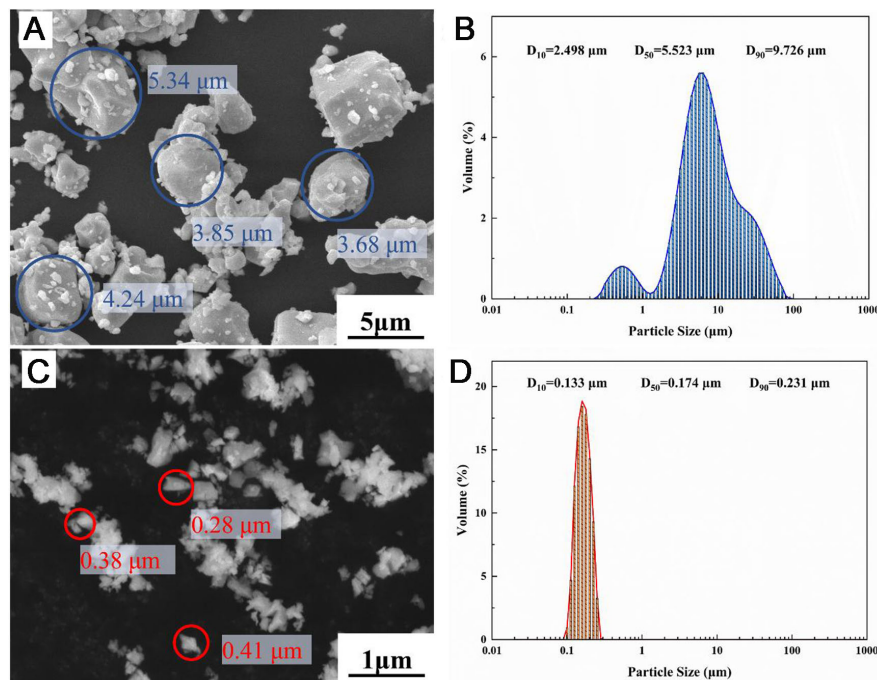


Figure 1. SEM of powder (A) and (B) before ball milling; (C) and (D) after ball milling. SEM: Scanning electron microscopy.

The specimens had to be divided into 10 mm × 10 mm × 1 mm pieces, and acetone was used to remove the silicone oil from the surface. The three-dimensional morphology of the PZT coating surface was observed using an atomic force microscope (AFM, Bruker Multimode 8), and the surface roughness of the samples was calculated. The elastic modulus and microhardness of PZT coatings were tested by using a nanoindenter (Anton Paar UNHT).

Electrical performance tests will be conducted on the upper and lower electrodes of the PZT coating. The PZT-coated substrate (SUS304) has excellent electrical conductivity and can be used directly as the bottom electrode. A platinum electrode with a 3 mm diameter was created on the coating surface using ion sputtering (LEICA EM SCD005, Germany). A HYJH-3-4 piezoelectric polarization system and a pressure resistance tester of type RK2671A were also used to polarize the PZT coating. The PZT coating was polarized at 120 °C for 10-60 min. Samples with a thickness of 40 μm were polarized at 60 kV/cm. While the impedance analyzer (Agilent 4294A, USA) was used to test the dielectric constant and dielectric loss of the material, the piezoelectric coefficient of the PZT coating was measured using a ZJ-4AN quasi-static d_{33} measuring equipment. The TF analyzer 2000E ferroelectric analyzer was also utilized to test the ferroelectric characteristics.

Preparation of PZT coating

In this experiment, PZT coating was made by PZT [$\text{Pb}(\text{Zr}_{0.52}\text{Ti}_{0.48})\text{O}_3$, 99.9%] powder. It is decided to use commercial PZT powder, which is produced by sintering Pb_3O_4 , ZrO_2 , and TiO_2 in a specific ratio at high temperatures. Particles of micron size were produced by mechanically crushing the sintered PZT ceramics. As shown in Figure 1A, the crushed PZT powder particles showed an irregular shape, and the size of the powder particles was about 5 μm. Figure 1B shows its corresponding powder particle size distribution; the overall particles of the powder were divided into the range of 0.5-100 μm mainly, and the D50 was 5.523 μm. Due to the difficulty of depositing large powder particles on the surface of the substrate during the spraying process and the serious erosion effect on the substrate, the VCS system requires a powder particle size of

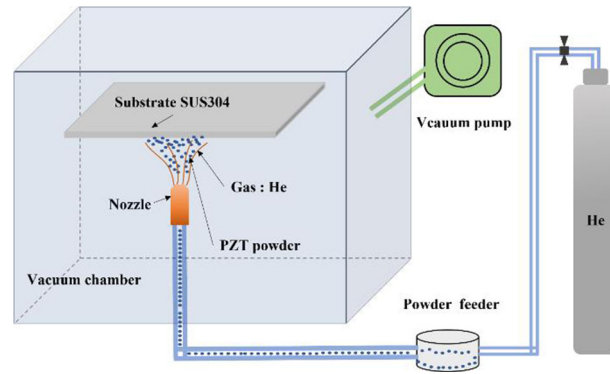


Figure 2. Schematic diagram of vacuum cold spraying. PZT: Lead zirconate titanate, $\text{Pb}(\text{Zr}, \text{Ti})\text{O}_3$.

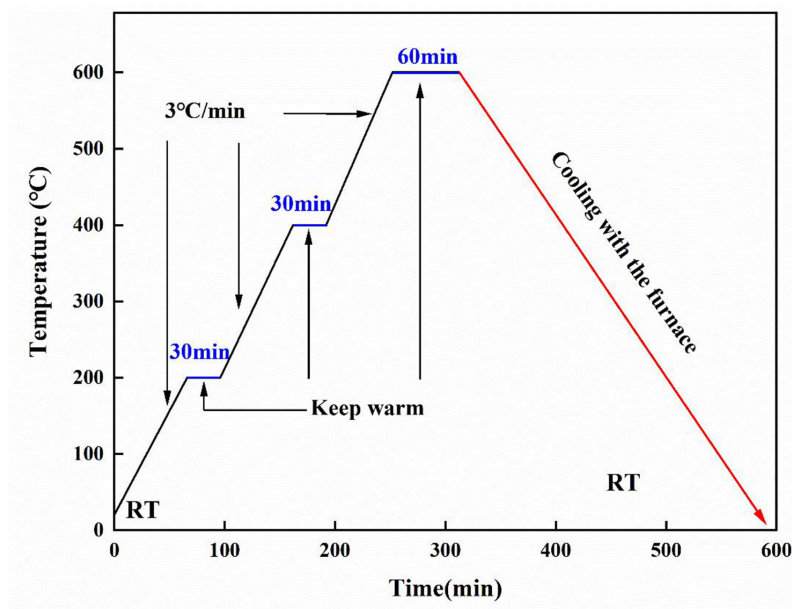


Figure 3. Heat treatment process. RT: Room temperature.

less than $2\ \mu\text{m}$ to be sprayed^[24]. Therefore, the above mechanically crushed PZT powder was subjected to a ball milling process [Table 1]. Figure 1C and D depicts the SEM images and the particle size distribution of the powder following ball milling. The ball milling process significantly reduces and evens out the powder particle size. The D50 value of $0.174\ \mu\text{m}$ of the powder meets the parameters of the VCS experiment.

As shown in Figure 2, the VCS system was used to create the PZT piezoelectric coating in this study. This system is primarily composed of a vacuum chamber, a powder feeding system, a gas supply system, a nozzle, and other parts^[25]. Through the powder feeding system, the VCS system produces an aerosol by mixing micro- and nano-sized PZT powder with the carrier gas provided by a He gas source. When the powder particles strike the surface of the substrate at high speed as a result of the aerosol's acceleration by the nozzle in the vacuum chamber, they are shattered and extruded to form a thin film under the pressure of the subsequent particles^[26-28].

Table 1. Ball milling process parameters

| Parameter | Value |
|------------------------|----------------------------|
| Ball milling jars | ZrO ₂ |
| Milling balls | ZrO ₂ ; 2, 5 mm |
| Dispersant | Anhydrous ethanol |
| Ball-to-material ratio | 10:1 |
| Rotating speed | 200 r/min |

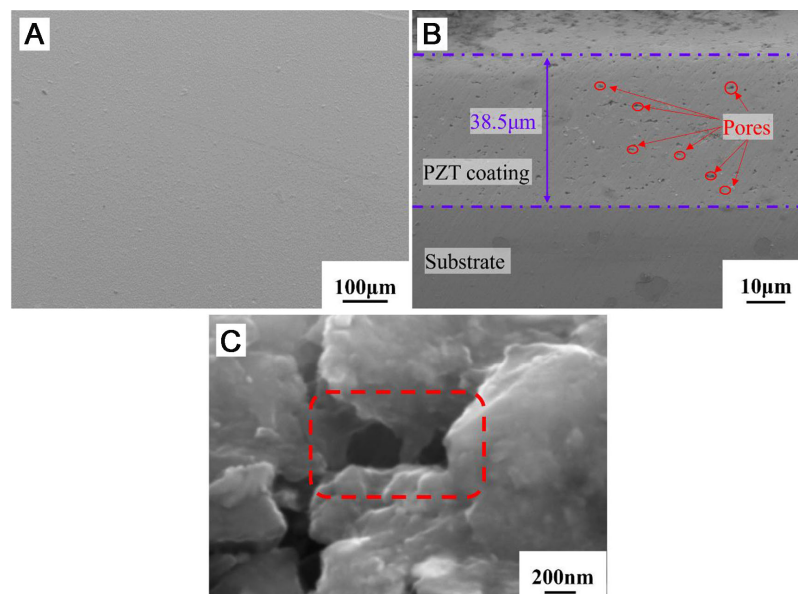


Figure 4. Microscopic morphology of the PZT coating. (A) Surface morphology; (B) Cross-sectional morphology; (C) Microstructure at high resolution. PZT: Lead zirconate titanate, Pb(Zr, Ti)O₃.

The PZT piezoelectric coatings in the present study were created by applying the VCS system in the thermal spray lab at Xi'an Jiaotong University. The spraying substrate is a SUS304 substrate with dimensions of 60 mm × 10 mm × 3 mm, in accordance with the spraying requirements of the VCS equipment and fixture installation requirements. Before the spraying, the sealing of the vacuum chamber must be verified, and the samples must be cleaned with ultrasonic energy and heated to promote the deposition of sprayed particles. Table 2 displays the procedure parameters that were employed in this study.

The PZT coating must be annealed after application to enhance its overall crystallinity, increase the grain size, and improve the electrical properties. The annealing procedure is shown in Figure 3 to guarantee the consistent and gradual release of internal stress in the PZT coating. The insulation is maintained at 200 °C, 400 °C for 30 min, and then 600 °C for 60 min, with the heating rate set at 3 °C/min.

RESULTS AND DISCUSSIONS

PZT coating surface and cross-section morphology

Figure 4 depicts the microscopic microstructure of PZT coating. As seen in Figure 4A, the PZT coating is of good quality with a smooth surface, a dense structure, and no evident flaws such as cracking or peeling. Figure 4B shows the cross-sectional morphology of the PZT coating with a coating thickness of about 38.5 μm, which shows that the coating is densely aligned and tightly bonded to the substrate without fracture defects. Figure 4C shows the internal microstructure of the PZT coating at high resolution. It can be

Table 2. Spraying parameters

| Deposition parameters | Vacuum chamber pressure | He gas flow rate | Mixture flow rate | Spray distance | Scanning speed | Nozzle size | Deposition temperature |
|-----------------------|-------------------------|------------------|-------------------|----------------|----------------|-------------|------------------------|
| Value | 60 ± 15 Pa | 2.5 L/min | 4 L/min | 8 mm | 5 mm/min | Φ 3.0 mm | 298 K |

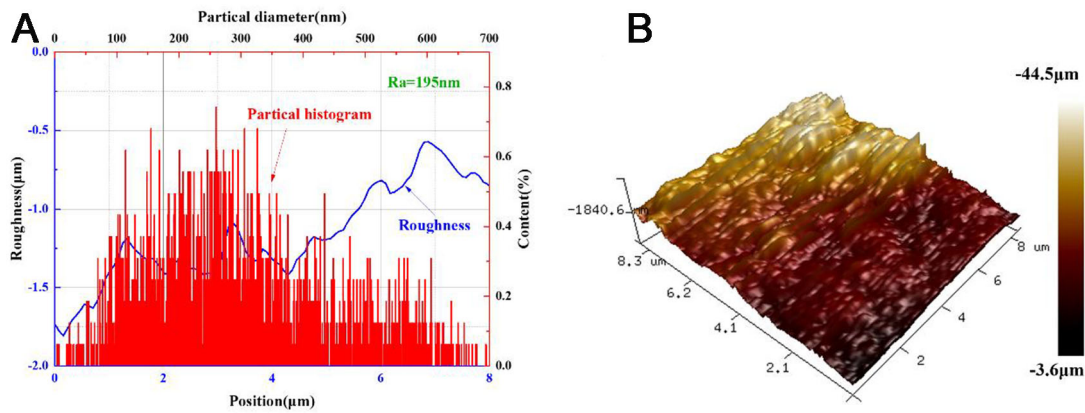


Figure 5. Three-dimensional morphology of the PZT coating. (A) Roughness and particle size distribution; (B) Three-dimensional morphology. PZT: Lead zirconate titanate, $\text{Pb}(\text{Zr}, \text{Ti})\text{O}_3$.

seen from the figure that the PZT coating is made of powder particles mechanically embedded, which is in line with the characteristics of coating formation by VCS technology. At the same time, it can be clearly seen that there are different sizes of pore structures between the powder particles and the powder particles, mainly due to the mechanical embedding of the powder particles cannot be completely matched. The findings demonstrate the preparation of a high-quality PZT coating with good crystallinity and a smooth surface on the surface of SUS304, and they also demonstrate the significance of the coating in the electrical property measurement.

Three-dimensional morphology

Figure 5 depicts the three-dimensional morphology of PZT coating. As shown in Figure 5A, the surface profile curve of the PZT coating and the particle size distribution of the surface particles indicate that the particle size distribution of the surface particles of the coating ranges from 100–700 nm. The surface particles are mainly concentrated at about 250 nm, which is consistent with the particle size of the sprayed powder after ball milling treatment. The surface of the PZT coating is quite smooth and consistent, with a roughness Ra value of 195 nm, as illustrated in Figure 5B. Thus, it is clear that the surface of PZT coating is primarily made up of nanostructures with surface particles whose sizes are far bigger than variations in the surface profile. The submicron-sized powder is continuously refined through high-speed impact, crushing, and compaction on the substrate in the vertical direction, which encourages surface nanostructuring and results in a higher degree of densification in the direction perpendicular to the substrate than in the horizontal direction.

Nano-mechanical properties characterization

Figure 6 depicts the results of a nanoindentation test performed on the PZT coating's surface. The nanoindentation displacement-load curve of the PZT coating is shown in Figure 6A. The curve was measured three times to ensure the accuracy of the experiment, and the average value was taken. The PZT coating has a microhardness of around 1,510 Hv and an average elastic modulus of about 73.9 Gpa [Figure 6B]. It is evident that the PZT covering is extremely hard, has a dense internal structure, and has few imperfections such as porosity.

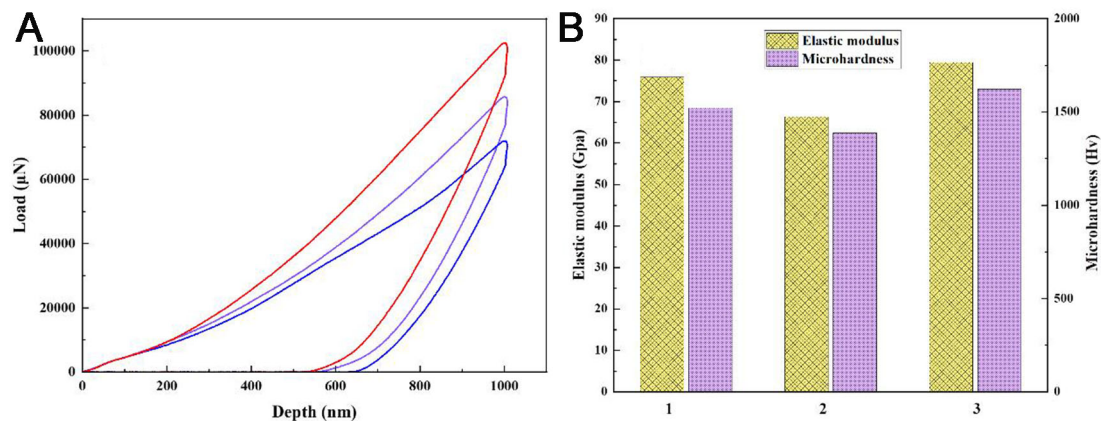


Figure 6. Nanoindentation analysis of the PZT coating. (A) Nanoindentation displacement load curve; (B) Elastic modulus and hardness. PZT: Lead zirconate titanate, $\text{Pb}(\text{Zr}, \text{Ti})\text{O}_3$.

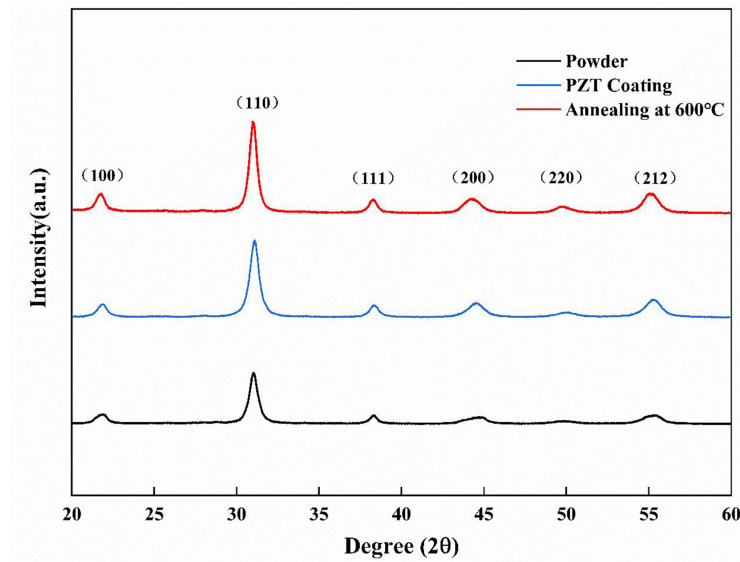


Figure 7. XRD patterns of PZT powder, coating, and coating after heat treatment at 600 °C. PZT: Lead zirconate titanate, $\text{Pb}(\text{Zr}, \text{Ti})\text{O}_3$; XRD: X-ray diffractometer.

Evolution of coating phase structure

Figure 7 shows the XRD patterns of PZT powder, coating, and coating following heat treatment at 600 °C. Compared to the (100) and (111) peaks, the (110) peak is sharper^[29,30]. Since the XRD diffraction peaks of the coating and the powder are so similar, it is clear that the PZT coating preserves the powder's lattice structure. The XRD diffraction data demonstrate that the PZT powder and coating both exhibit a typical tetragonal perovskite structure and that the phase structure was unaffected by the spraying process^[31]. This is primarily because the room temperature deposition properties of VCS prevent the prepared material from going through phase transformation despite the high temperature and pressure created at the time of powder particle impact. However, following the heat treatment, the intensity of all of the PZT coating's diffraction peaks significantly increased, indicating that flaws such as lattice distortion brought on by

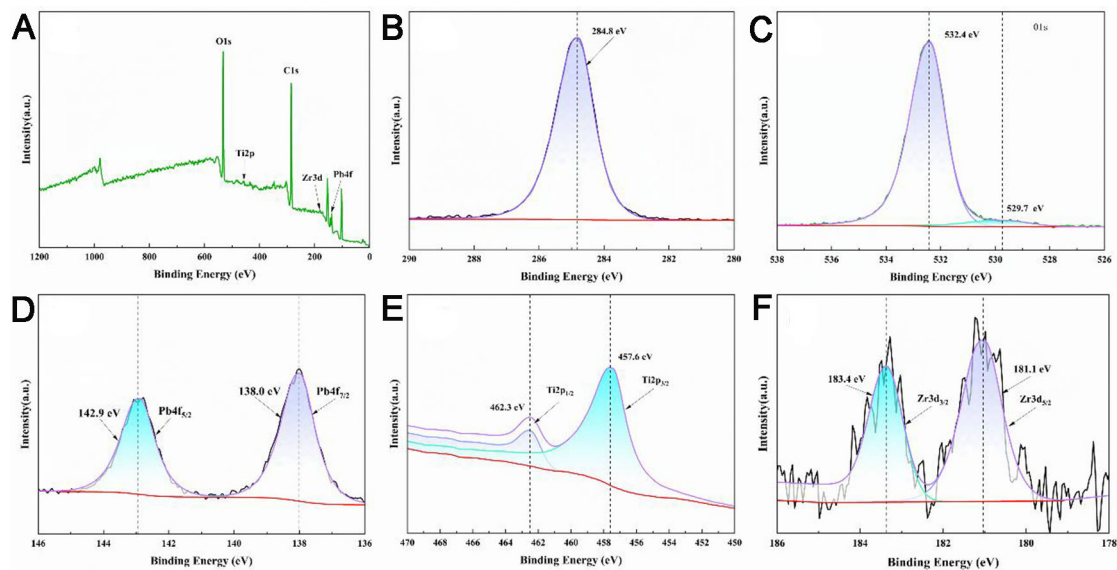


Figure 8. XPS survey spectra of the PZT coating (A) XPS full spectrum; (B)–(F) C, O, Pb, Ti, and Zr spectrum. PZT: Lead zirconate titanate, $\text{Pb}(\text{Zr}, \text{Ti})\text{O}_3$; XPS: Xi photoelectron spectrometer.

powder impact in the PZT coating were partially fixed, and the PZT coating's overall crystallinity was improved. The PZT coating treated at 600 °C also displayed a typical tetragonal phase structure in the XRD diffraction peaks. It is advantageous to enhance the PZT coating's ferroelectric, dielectric, and piezoelectric properties^[32–34].

Valence analysis of coating elements

By using XPS analysis, the element chemical state and valence state of the PZT coating were evaluated. **Figure 8A** shows the entire XPS spectrum of the PZT coating. **Figure 8B–F** displays the results of each elemental spectrum for C, O, Pb, Ti, and Zr. As can be shown in **Figure 8B**, the 284.8 eV C1s binding energy is regarded as a surface contaminant on the C-peak PZT coating and an unidentified hydrocarbon of the XPS instrument. **Figure 8C** shows that the binding energy of oxygen in the coating's internal lattice is 529.7 eV, whereas the binding energy of oxygen adsorbed on the coating surface is 532.4 eV^[35–37]. There is just one stable chemical state of lead, as shown by the binding energies of $\text{Pb}4f_{7/2}$ and $\text{Pb}4f_{5/2}$ in **Figure 8D**, and there is no lead loss throughout processing. According to **Figure 8E**, $\text{Ti}2p_{3/2}$ has a binding energy of 457.6 eV, while $\text{Ti}2p_{1/2}$ has a binding energy of 462.3 eV. $\text{Zr}3d_{5/2}$ and $\text{Zr}3d_{3/2}$ had binding energies of 181.1 and 183.4 eV, respectively, according to **Figure 8F**. The experimental results show that Pb, Ti, or Zr do not change valence during the spray preparation process, further supporting the characteristics of vacuum cold spray vacuum room temperature deposition^[38,39].

PZT coating piezoelectric property

PZT coatings are polarized at 60 kV/cm for 10–60 min at 120 °C. **Figure 9** displays d_{33} of the PZT coating during different polarization times. The figure demonstrates that d_{33} of the PZT coating rises with the polarization time, reaching a maximum of 46 pC/N after 30 min. The PZT coating is formed by the crushing and extrusion accumulation of micro- and nano-powders, and there are some degrees of pores and other defects inside the coating. According to the space charge theory proposed by Okayazaki and Nagata, when a piezoelectric ceramic is polarized, the force exerted by the applied electric field on the domains is in the opposite direction to the force exerted on the space charge, thus hindering the migration and rotation of the domain walls^[40]. The presence of pores in the coating introduces a space charge field that affects the polarizability of the coating, which, in turn, affects the piezoelectric properties of the coating.

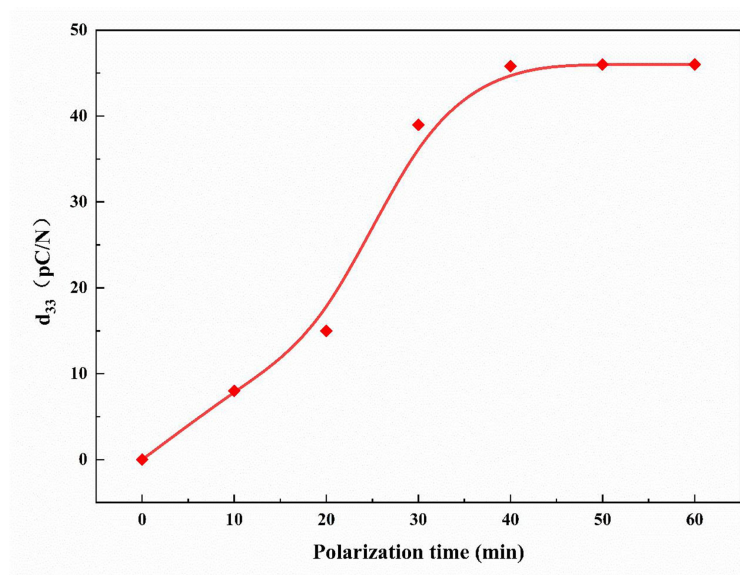


Figure 9. d_{33} of the PZT coating during different polarization times. PZT: Lead zirconate titanate, $\text{Pb}(\text{Zr}, \text{Ti})\text{O}_3$.

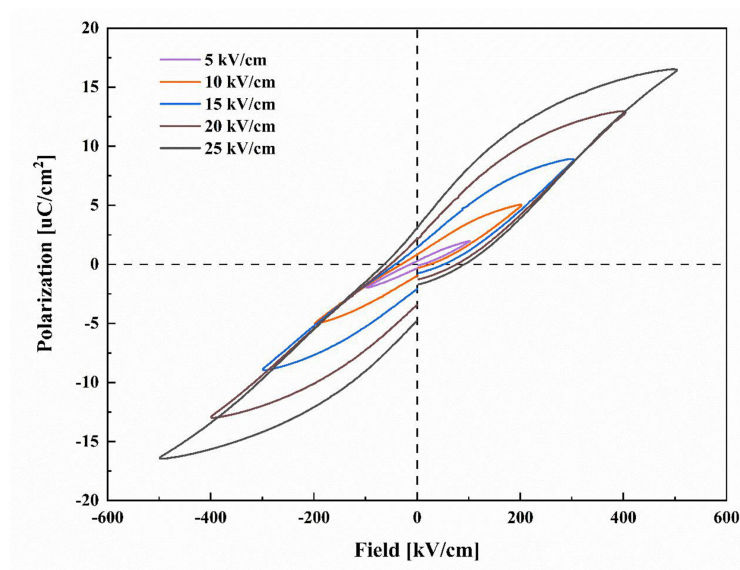


Figure 10. P-E hysteresis loops of the PZT coating at room temperature with different electric fields at 1 kHz. PZT: Lead zirconate titanate, $\text{Pb}(\text{Zr}, \text{Ti})\text{O}_3$.

PZT coating ferroelectric property

Figure 10 shows the hysteresis loops of PZT coatings at room temperature with different electric fields at 1 kHz. The results show that the electric hysteresis loops of PZT coating have a typical loop shape, which indicates that the coating has ferroelectric properties^[41,42]. The saturation polarization values (P_s) of PZT coating at different electric fields were 1.9, 4.9, 8.8, 12.8, and 16.2 $\mu\text{C}/\text{cm}^2$, respectively; and the coercive fields (E_c) of PZT coating were 8.3, 20.4, 36.1, 50.0, and 59.3 kV/cm. In the studied range (before saturation), the remanent polarization (P_r) and E_c of PZT coating increased with the increase of the applied

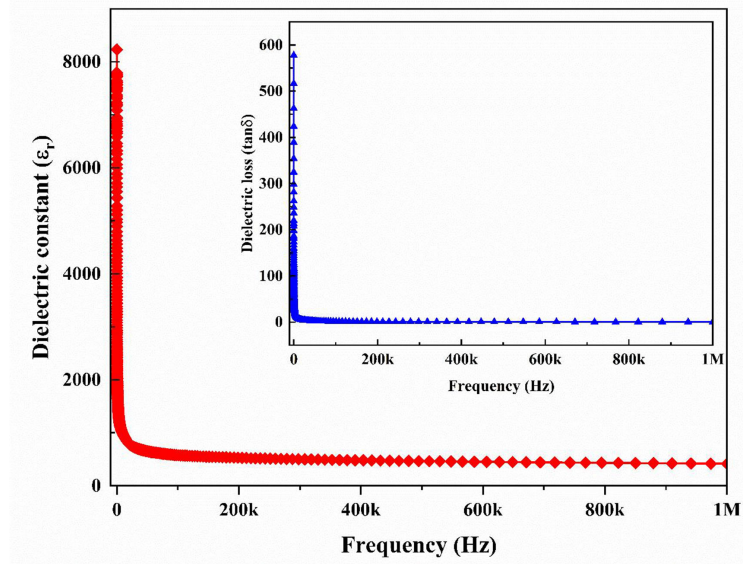


Figure 11. Frequency dependence of dielectric loss and dielectric constant of the PZT coating. PZT: Lead zirconate titanate, $\text{Pb}(\text{Zr}, \text{Ti})\text{O}_3$.

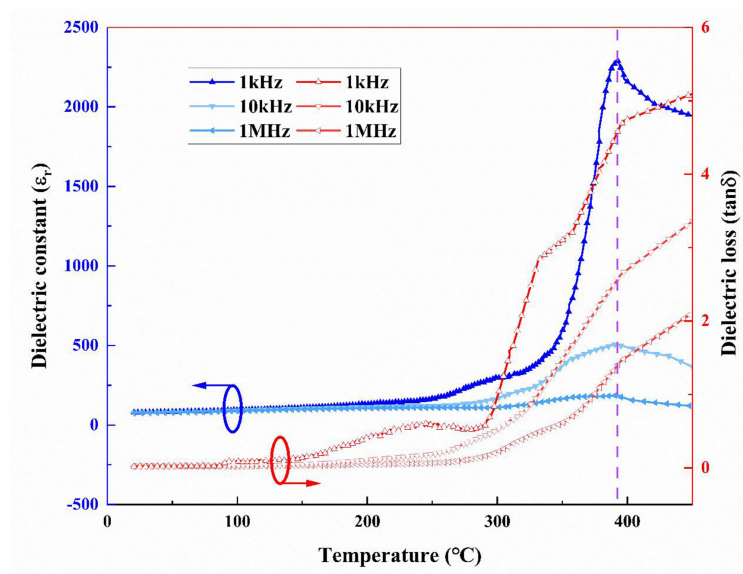


Figure 12. Temperature dependence of the dielectric constant and dielectric loss of the PZT coating at different frequencies. PZT: Lead zirconate titanate, $\text{Pb}(\text{Zr}, \text{Ti})\text{O}_3$.

electric field, as shown in [Figure 10](#). When the electric field is 25 kV/cm, PZT coating has good ferroelectric properties, and the hysteresis loop is relatively saturated with a maximum remanent polarization P_r of $3.1 \mu\text{C}/\text{cm}^2$ and a coercive field E_c of 59.3 kV/cm. However, the PZT coating is formed by crushing, extruding, and stacking micro- and nano-powders after accelerating them in a vacuum environment, so there are defects, such as pores and cracks, inside the coating, which lead to problems such as space charge polarization in the coating; so, the P-E hysteresis loops appear to be non-closed^[43,44].

PZT coating dielectric property

PZT coating dielectric spectrum

Figure 11 shows the frequency dependence of the dielectric constant and dielectric loss of PZT coating. From the figure, it is observed that the dielectric constant is unstable at low frequencies, and with the increase of frequency, the dielectric constant decreases rapidly before finally stabilizing. The dielectric constant/dielectric loss of PZT coating is about 425 (0.35). It is mainly due to the internal polarization process of the PZT coating, which is mainly caused by the combined effect of electron displacement polarization, ion displacement polarization, intrinsic electric dipole orientation polarization, and space charge polarization^[45]. As the frequency increases, the value of the dielectric constant decreases at high frequencies and eventually stabilizes to equilibrium due to the weakening of the space charge polarization effect^[46].

Dielectric temperature spectrum

Figure 12 shows the temperature dependence of the dielectric constant and dielectric loss of PZT coating at different frequencies. From the figure, it can be seen that the dielectric constant (ϵ_r) increases with increasing temperature at different frequencies, and the temperature at which the dielectric constant (ϵ_r) reaches its highest value is the Curie temperature (T_c) of the PZT coating. When the temperature approaches T_c , the ferroelectric phase in the PZT coating transitions towards the Paraelectric phase^[47]. The T_c of the PZT coating is 392.6 °C, and the maximum dielectric constant (ϵ_{max}) is 2,291 at 1 kHz.

In conclusion, the PZT piezoelectric ceramic coating was prepared on the SUS304 substrate by VCS, and the phase organization, microstructure morphology, and electrical properties were investigated.

1. According to XRD patterns, the PZT coating shows a typical tetragonal perovskite phase structure that does not change before or after spraying. The valence states of the elements included inside PZT materials do not change, according to the XPS study. This demonstrates that room-temperature deposition characteristics of VCS technology provide a non-destructive way to prepare PZT coatings.
2. The PZT coating surface is uniform and smooth, with a surface roughness of about 195 nm. The PZT coating has an elastic modulus of around 73.9 GPa, and its microhardness is about 1,510 Hv. With the exception of a small percentage of porosity, the PZT coating's overall structure is sound.
3. The piezoelectric coefficient d_{33} of the PZT coating is about 46 pC/N. The maximum saturation polarization of the PZT coating is 16.2 $\mu\text{C}/\text{cm}^2$, the remnant polarization is 3.1 $\mu\text{C}/\text{cm}^2$, and the coercive field is 59.3 kV/cm, which exhibits a certain ferroelectricity. The dielectric constant/dielectric loss of the PZT coating is about 425/0.35. The T_c of the PZT coating is 392.6 °C, which improves the dielectric constant and the dielectric loss. It can be seen that the PZT coatings prepared by VCS have a certain degree of electrical properties, which provides a new method to establish and improve the piezoelectric ceramic coating system for monitoring the damage state of parts at a later stage.

DECLARATIONS

Author's contributions

Conceptualization: Zhu H, Xing Z

Formal analysis: Zhu H, Mi Q

Methodology: Dong H

Data curation, writing - original draft: Zhu H

Writing - review and editing: Huang Y

Supervision: Guo W

Availability of data and materials

Not applicable.

Financial support and sponsorship

The paper was financially supported by the General program of the National Natural Science Foundation of China (Grant No. 52275227). The authors gratefully acknowledge the National Key Laboratory for Remanufacturing and Shanghai University for supporting all the experiments.

Conflicts of interest

All authors declared that there are no conflicts of interest.

Ethical approval and consent to participate

Not applicable.

Consent for publication

Not applicable.

Copyright

© The Author(s) 2023.

REFERENCES

1. Zhu S, Du W, Wang X, Han G, Ren Z, Zhou K. Advanced additive remanufacturing technology. *Chin J Mech Eng Addit Manuf Front* 2023;2:100066. [DOI](#)
2. Xu BS. The remanufacturing engineering and automatic surface engineering technology. *Key Eng Mater* 2008;373-4:1-10. [DOI](#)
3. Yin J, Chen S, Wong VK, Yao K. Thermal sprayed lead-free piezoelectric ceramic coatings for ultrasonic structural health monitoring. *IEEE Trans Ultrason Ferroelectr Freq Control* 2022;69:3070-80. [DOI](#)
4. Huang J, Yao M, Yao X. A novel approach to improving the electromechanical properties of PZT-based piezoelectric ceramics via a grain coating modification strategy. *Ceram Int* 2021;47:16294-302. [DOI](#)
5. Chen S, Tan CKI, Tan SY, Guo S, Zhang L, Yao K. Potassium sodium niobate (KNN)-based lead-free piezoelectric ceramic coatings on steel structure by thermal spray method. *J Am Ceram Soc* 2018;101:5524-33. [DOI](#)
6. Xu G, Ren ZH, Weng WJ, Du PY, Han GR. Synthesis of perovskite $\text{Pb}(\text{Zr}_{0.52}\text{Ti}_{0.48})\text{O}_3$ (PZT) powders by a modified coprecipitation method. *Key Eng Mater* 2007;280-3:627-30. [DOI](#)
7. Akedo J, Lebedev M. Microstructure and electrical properties of lead zirconate titanate ($\text{Pb}(\text{Zr}_{52}/\text{Ti}_{48})\text{O}_3$) thick films deposited by aerosol deposition method. *Jpn J Appl Phys* 1999;38:5397. [DOI](#)
8. Guo R, Cross LE, Park SE, Noheda B, Cox DE, Shirane G. Origin of the high piezoelectric response in $\text{PbZr}_{1-x}\text{Ti}_x\text{O}_3$. *Phys Rev Lett* 2000;84:5423-6. [DOI](#) [PubMed](#)
9. Schäufele AB, Härdtl KH. Ferroelastic properties of lead zirconate titanate ceramics. *J Am Ceram Soc* 1996;79:2637-40. [DOI](#)
10. Breboel K, Pedersen L, Wolny W. 3-3 composites with different ceramic phases-lead titanate zirconate and lead titanate. In: IEEE International Symposium on Applications of Ferroelectrics; 1990 Jun 06-08; Urbana-Champaign, IL, USA. IEEE; 2002. p. 18-21. [DOI](#)
11. Santos DM, Simões AZ, Zaghete MA, Paiva-santos CO, Varela JA, Longo E. Synthesis and electrical characterization of tungsten doped $\text{Pb}(\text{Zr}_{0.53}\text{Ti}_{0.47})\text{O}_3$ ceramics obtained from a hybrid process. *Mater Chem Phys* 2007;103:371-4. [DOI](#)
12. Gupta R, Verma S, Singh D, Singh K, Bamzai KK. Effect of Ni/Nb on structure, electrical and ferroelectric properties of 0.5PNN-0.5PZT ceramics. *Process Appl Ceram* 2015;9:1-9. [DOI](#)
13. Monga S, Sharma N, Mehan N, Mishra YK, Singh A. Qualitative analysis of PZT (52/48) MPB using different synthesis methods. *Ceram Int* 2022;48:31111-20. [DOI](#)
14. Liu Z, Xing Z, Wang H, Cui X, Jin G, Chen S. Fabrication and post heat treatment of 0.5Pb ($\text{Mg}_{1/3}\text{Nb}_{2/3}$) O_3 -0.5Pb($\text{Zr}_{0.48}\text{Ti}_{0.52}$) O_3 coatings by supersonic plasma spray. *J Eur Ceram* 2017;37:3511-9. [DOI](#)
15. Krupanidhi SB, Maffei N, Sayer M, El-Assal K. rf planar magnetron sputtering and characterization of ferroelectric $\text{Pb}(\text{Zr,Ti})\text{O}_3$ films. *J Appl Phys* 1983;54:6601-9. [DOI](#)
16. Seveno R, Limousin P, Averty D, Chartier JL, Le Bihan R, Gundel HW. Preparation of multi-coating PZT thick films by sol-gel

- method onto stainless steel substrates. *J Eur Ceram Soc* 2000;20:2025-8. DOI
17. Fan SQ, Li CJ, Li CX, Liu GJ, Yang GJ, Zhang LZ. Preliminary study of performance of dye-sensitized solar cell of nano-TiO₂ coating deposited by vacuum cold spraying. *Mater Trans* 2006;47:1703-9. DOI
 18. Akedo J, Ichiki M, Kikuchi K, Maeda R. Jet molding system for realization of three-dimensional micro-structures. *Sens Actuator A Phys* 1998;69:106-12. DOI
 19. Chun DM, Kim CS, Choi JO, Lee GY, Lee CS, Ahn SH. Multilayer deposition of ceramic and metal at room temperature using nanoparticle deposition system (NPDS) and planarization process. *Int J Adv Manuf Technol* 2014;72:41-6. DOI
 20. Moridi A, Hassani-Gangaraj SM, Guagliano M, Dao M. Cold spray coating: review of material systems and future perspectives. *Surf Eng* 2014;30:369-95. DOI
 21. Akedo J. Aerosol deposition of ceramic thick films at room temperature: densification mechanism of ceramic layers. *J Am Ceram Soc* 2006;89:1834-9. DOI
 22. Chun DM, Ahn SH. Deposition mechanism of dry sprayed ceramic particles at room temperature using a nano-particle deposition system. *Acta Mater* 2011;59:2693-703. DOI
 23. Akedo J. Room temperature impact consolidation (RTIC) of fine ceramic powder by aerosol deposition method and applications to microdevices. *J Therm Spray Tech* 2008;17:181-98. DOI
 24. Akedo J, Lebedev M. Powder preparation in aerosol deposition method for lead zirconate titanate thick films. *Jpn J Appl Phys* 2002;41:6980. DOI
 25. Ma K, Li CJ, Li CX. Narrow and thin copper linear pattern deposited by vacuum cold spraying and deposition behavior simulation. *J Therm Spray Tech* 2021;30:571-83. DOI
 26. Patil DR, Annapureddy V, Kaarthik J, Thakre A, Akedo J, Ryu J. Piezoelectric thick film deposition via powder/granule spray in vacuum: a review. *Actuators* 2020;9:59. DOI
 27. Fan SQ, Yang GJ, Li CJ, Liu GJ, Li CX, Zhang LZ. Characterization of microstructure of nano-TiO₂ coating deposited by vacuum cold spraying. *J Therm Spray Technol* 2006;15:513-7. DOI
 28. Wang YY, Liu Y, Li CJ, Yang GJ, Kusumoto K. Electrical and mechanical properties of nano-structured TiN coatings deposited by vacuum cold spray. *Vacuum* 2012;86:953-9. DOI
 29. Chen X, Qiao X, Zhang L, et al. Temperature dependence of ferroelectricity and domain switching behavior in Pb(Zr_{0.3}Ti_{0.7})O₃ ferroelectric thin films. *Ceram Int* 2019;45:18030-6. DOI
 30. Shakeri A, Abdizadeh H, Golobostanfard MR. Effects of calcination parameters on the microstructure and morphology of PZT nanoparticles prepared by modified sol-gel method. *Adv Mater Res* 2012;576:326-9. DOI
 31. Surowiak Z, Kupriyanov MF, Czekaj D. Properties of nanocrystalline ferroelectric PZT ceramics. *J Eur Ceram Soc* 2001;21:1377-81. DOI
 32. Damjanovic D, Taylor DV, Setter N. Crystal structure and texture effects on piezoelectric and dielectric properties of PZT thin films. *MRS Proc* 1999;596:529-34. DOI
 33. Li P, Zhai J, Zeng H, Shen B, Li W, Zhao K. Crystallographic orientation dependence of piezoelectric and dielectric properties of BNT-based thin films. *J Eur Ceram Soc* 2016;36:3139-45. DOI
 34. Oikawa T, Aratani M, Funakubo H, Saito K, Mizuhira M. Composition and orientation dependence of electrical properties of epitaxial Pb(ZrxTi_{1-x})O₃ thin films grown using metalorganic chemical vapor deposition. *J Appl Phys* 2004;95:3111-5. DOI
 35. Singh S, Kaur A, Kaur P, Singh L. Oxygen vacancies induced anomalies in the structural, ferroelectric and magnetic behaviour of sol-gel derived LaCoO₃ modified Na_{0.5}Bi_{0.5}TiO₃ ceramics. *Mater Chem Phys* 2022;279:125754. DOI
 36. Mar GL, Timbrell PY, Lamb RN. Factors influencing the chemical vapor deposition of oriented ZnO films using zinc acetate. *Chem Mater* 1995;7:1890-6. DOI
 37. Samantaray KS, Amin R, Ayaz S, et al. Room temperature magneto-dielectric coupling in the CaMnO₃ modified NBT lead-free ceramics. *Appl Phys A* 2023;129:237. DOI
 38. Wang X, Wang S, Qi L, et al. Enhanced dielectric and piezoelectric properties of RF sputtered Pb(Zr_{0.60}Ti_{0.40})O₃ thin films deposited on sol-gel derived Pb_{1+x}(Zr_{0.40}Ti_{0.60})O₃ seed layer with various lead contents. *J Alloys Compd* 2019;807:151660. DOI
 39. Ctibor P, Pala Z, Boldyryeva H, Sedláček J, Kmetik V. Microstructure and properties of plasma sprayed lead zirconate titanate (PZT) ceramics. *Coatings* 2012;2:64-75. DOI
 40. Okazaki K, Nagata K. Effects of grain size and porosity on electrical and optical properties of PLZT ceramics. *J Am Ceram Soc* 1973;56:82-6. DOI
 41. Singh P, Jha RK, Goswami M, Singh BR. Integration of perovskite Pb[Zr_{0.35}Ti_{0.65}]O₃/HfO₂ ferroelectric-dielectric composite film on Si substrate. *Microelectron Int* 2020;37:155-62. DOI
 42. Liu Y, Yang T, Wang H. Effect of La doping on structure and dielectric properties of PLZST antiferroelectric ceramics. *J Mater Sci Mater Electron* 2020;31:1509-14. DOI
 43. Zahn M. Physics of dielectrics for the engineer: by Roland Coelho, *Fundamental Studies in Engineering*, Vol. 1, Elsevier, Amsterdam, 1978, xi + 175 pages, Price US \$ 40.00/Dfl. 90.00, ISBN 0-444-41755-9. *J Electrostat* 1979;6:381-5. DOI
 44. Xi XJ, Wang SY, Liu WF, et al. Modulation of electric conduction in La-Mg codoped multiferroic BiFeO₃ ceramics. *J Alloy Compd* 2014;603:224-9. DOI
 45. Barick BK, Mishra KK, Arora AK, Choudhary RNP, Pradhan DK. Impedance and Raman spectroscopic studies of (Na_{0.5}Bi_{0.5})TiO₃. *J Phys D Appl Phys* 2011;44:355402. DOI

46. Pansara PR, Raval PY, Vasoya NH, Dolia SN, Modi KB. Intriguing structural and magnetic properties correlation study on Fe³⁺-substituted calcium-copper-titanate. *Phys Chem Chem Phys* 2018;20:1914-22. [DOI](#)
47. Ramesh R, Aggarwal S, Auciello O. Science and technology of ferroelectric films and heterostructures for non-volatile ferroelectric memories. *Mater Sci Eng R Rep* 2001;32:191-236. [DOI](#)